1.0

1.1

1.25 1.4 1.6

2.8 2.5

3.2 2.2

3.6

4.0 2.0

1.8

MICROCOPY RESOLUTION TEST CHART

NATIONAL BUREAU OF STANDARDS 1963 A

TECHNICAL REPORT RH-76-7

MEDIUM HOMOGENEITY IN A CHEMICAL
LASER CAVITY USING A LATERAL SHEARING
INTERFEROMETER

Army High Energy Laser Directorate
US Army Missile Research, Development
and Engineering Laboratory

January 1976

Approved for public release; distribution unlimited

U.S. ARMY MISSILE COMMAND
Redstone Arsenal, Alabama

D D C

RECEIVED

AUG 8 1977

RECEIVED

B

DISPOSITION INSTRUCTIONS

DISCLAIMER

TRADE NAMES

REPORT DOCUMENTATION PAGE		READ INSTRUCTIONS BEFORE COMPLETING FORM
1. REPORT NUMBER RH-76-7	2. GOVT ACCESSION NO.	3. RECIPIENT'S CATALOG NUMBER
4. TITLE (and Subtitle) Medium Homogeneity in a Chemical Laser Cavity Using a Lateral Shearing Interferometer		5. TYPE OF REPORT & PERIOD COVERED Technical Report
		6. PERFORMING ORG. REPORT NUMBER RH-76-7
7. AUTHOR(s) R. William Jones, W. Lavaughn Hales		8. CONTRACT OR GRANT NUMBER(s)
9. PERFORMING ORGANIZATION NAME AND ADDRESS Commander US Army Missile Command ATTN: AMSMI-RH Redstone Arsenal, Alabama 35809		10. PROGRAM ELEMENT, PROJECT, TASK AREA & WORK UNIT NUMBERS (DA) 1X363314D093 AMCMS Code 633314.12.26000
11. CONTROLLING OFFICE NAME AND ADDRESS Commander US Army Missile Command ATTN: AMSMI-RPR Redstone Arsenal, Alabama 35809		12. REPORT DATE January 1976
		13. NUMBER OF PAGES 26
14. MONITORING AGENCY NAME & ADDRESS(If different from Controlling Office)		15. SECURITY CLASS. (of this report) UNCLASSIFIED
		15a. DECLASSIFICATION/DOWNGRADING SCHEDULE

16. DISTRIBUTION STATEMENT (of this Report)

Cleared for public release; distribution unlimited.

17. DISTRIBUTION STATEMENT (of the abstract entered in Block 20, If different from Report)

18. SUPPLEMENTARY NOTES

19. KEY WORDS (Continue on reverse side if necessary and identify by block number)

Chemical laser cavity
Lateral shearing interferometer
Flow visualization
Holography

20. ABSTRACT (Continue on reverse side if necessary and identify by block number)

    This report is a study of recent chemical laser tests conducted at the US Army Missile Command, Redstone Arsenal, Alabama which incorporated a real-time flow visualization diagnostic for observing flow field conditions in the chemical laser cavity. Of particular interest in this study is the use of a holographically constructed lateral shearing interferometer to calculate refractive index variations in the flow.

DD FORM 1 JAN 73 1473   EDITION OF 1 NOV 65 IS OBSOLETE

402 268

CONTENTS

1. Introduction

Recent chemical laser tests at the US Army Missile Command (MICOM) Redstone Arsenal, Alabama have incorporated a real-time flow visualization diagnostic for observing flow field conditions in the chemical laser cavity. Of particular interest was the use of a holographically constructed lateral shearing interferometer to calculate refractive index variations in the flow.

The chemical laser utilized in this series of tests is the modular subscale breadboard evaluation device (MSBED) [1]. The device was operated as a chemical transfer laser in which excited DF molecules transfer their vibrational energy to CO_2 molecules.

The MSBED is broken down into four basic units (Figure 1): the combustor, nozzle bank, cavity, and diffuser. The combustor supplies F atoms to the primary nozzles by burning hydrogen in an excess of fluorine. It is regeneratively cooled, the injector part being a hyperthin platelet concept developed by Aerojet [2]. Nominal combustor pressure was approximately 34 psia with greater than 90% dissociation of excess fluorine molecules.

NOTE: Dimensions given in inches.
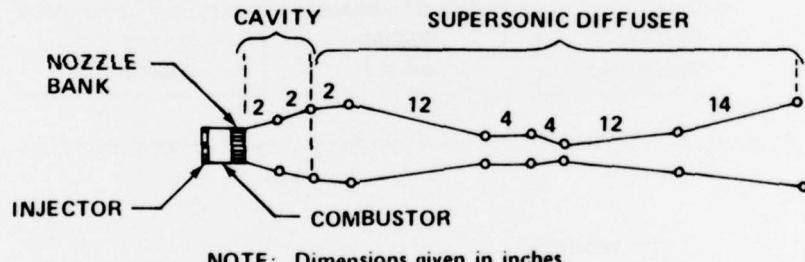
Figure 1. Schematic of the modular subscale breadboard evaluation device (MSBED).

The nozzle bank is a supersonic two-dimensional slit concept with 40 secondary nozzles alternating with 39 primaries [3]. A schematic of a nozzle pair (one primary, two secondaries) is shown in Figure 2. The CO_2 is bled into the primary upstream of the throat. Overall exit dimensions of the nozzle bank is 2-in. high by 8-in. long with slits arranged vertically.

The laser cavity has a pair of movable plates, top and bottom, which serve as shrouds for confinement of laser gases (Figure 3). Shroud angles are adjustable from 0° to 12°. Purge boxes on the cavity sides hold the windows which permit observation of flow in the cavity. Nitrogen purge in the boxes minimize the corrosive effects of HF and DF recirculation near the windows.
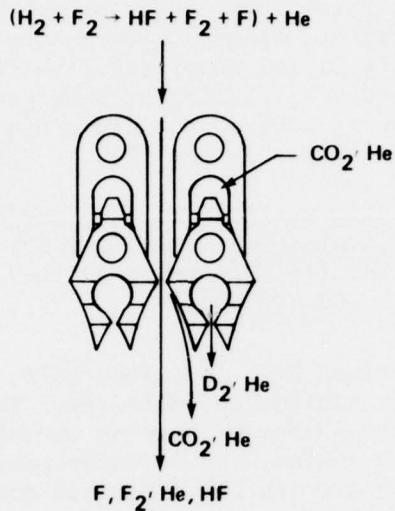
3

Figure 2. Split diluent boundary layer bleed nozzles.
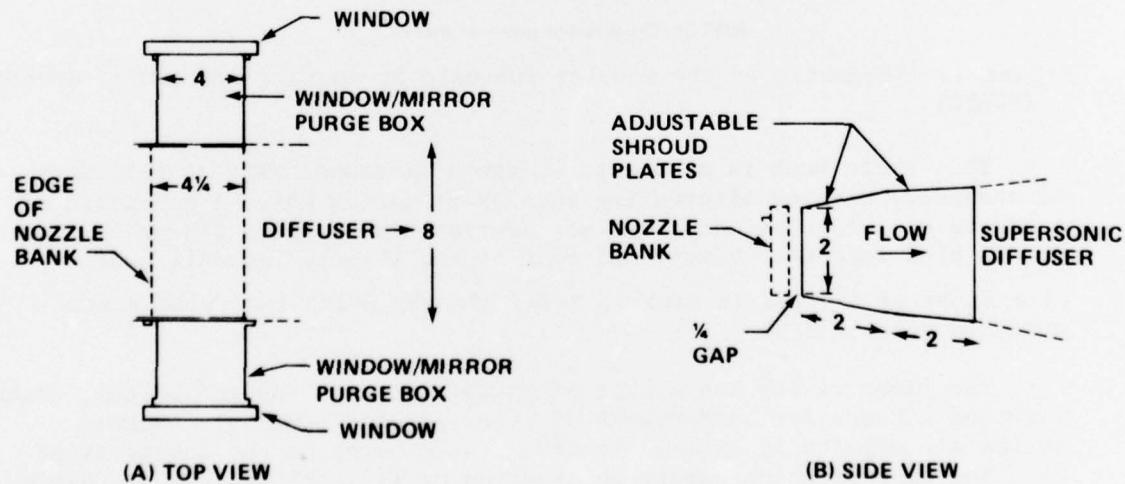
NOTE: Dimensions given in inches.

Figure 3. Chemical laser cavity.

For pressure recovery demonstration, the spent laser gases exit into a supersonic diffuser. The diffuser has movable top and bottom walls similar to the cavity in configuration [1]. Each is partitioned into 8 hinged plates of lengths 2, 12, 4, 4, and 12 in. The plates are adjustable and form a metal-to-metal seal with the vertical sides of the diffuser. From this point, the gases exit through a backpressure valve into a vacuum sink.

2. Flow Visualization Apparatus

a. Test Configuration

A schematic of the flow visualization setup is shown in Figure 4. A helium-neon laser coupled with a spatial filter provide a clean (spatially coherent) expanding beam of light. A large 6-in. lens is placed with its infinity focus at the pinhole of the spatial filter which gives a large collimated beam. The light then passes through a window into the flow field and exits through another window on the opposite side of the chemical laser cavity. A similar 6-in. lens is then used to focus the light to a point at which the various flow visualization techniques are applied. A knife edge is shown in the figure. This will give a Schlieren presentation of the flow field, the direction of sensitivity dependent upon the orientation of the knife edge. With the knife edge removed completely, the recorded image of the flow field is a shadowgraph. A pinhole placed at the focus will give an image having radial sensitivity. A holographic plate is placed at (or near) the focus for viewing of shearing interferograms. A small lens is used to focus the image onto a TV or motion picture camera. For TV viewing, a video tape recorder with monitor is used to record the test. Figures 5 and 6 show the test equipment in place. A front view of the chemical laser is seen in Figure 5 with the helium-neon on the right and TV camera on the left. Figure 6 shows the video recorder and monitor in place in the laser control room.
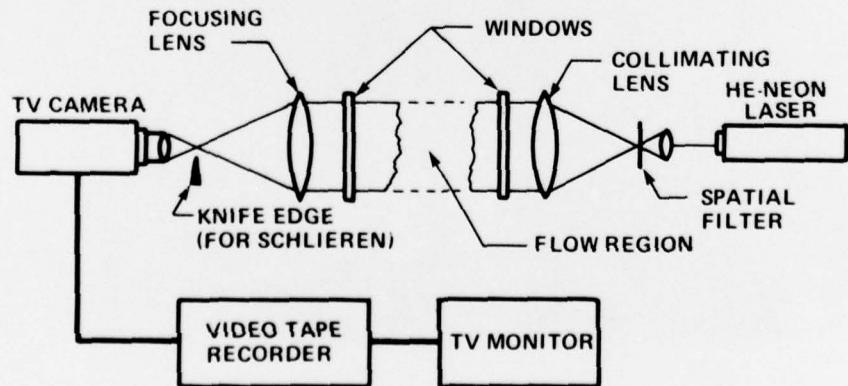
Figure 4. Real-time flow visualization.
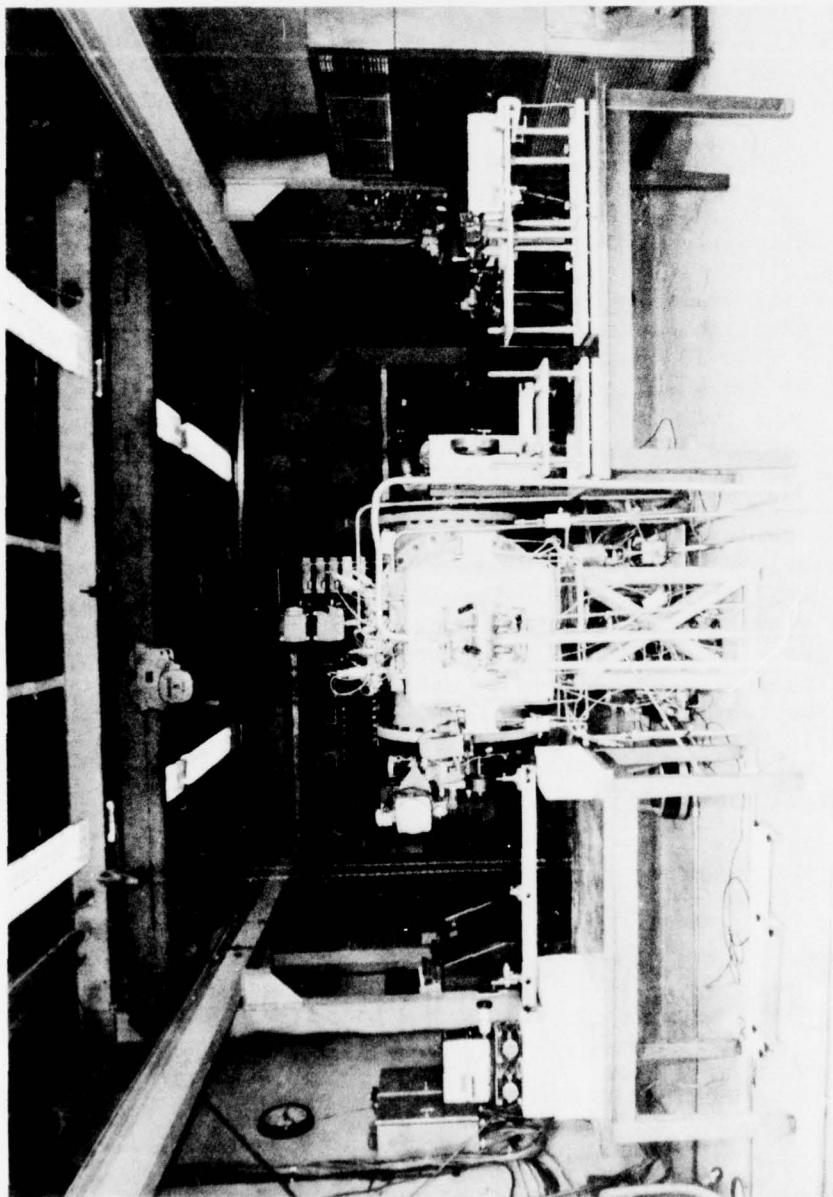
Figure 5. Operational test configuration. (The chemical laser hardware is in the center of the photograph.)
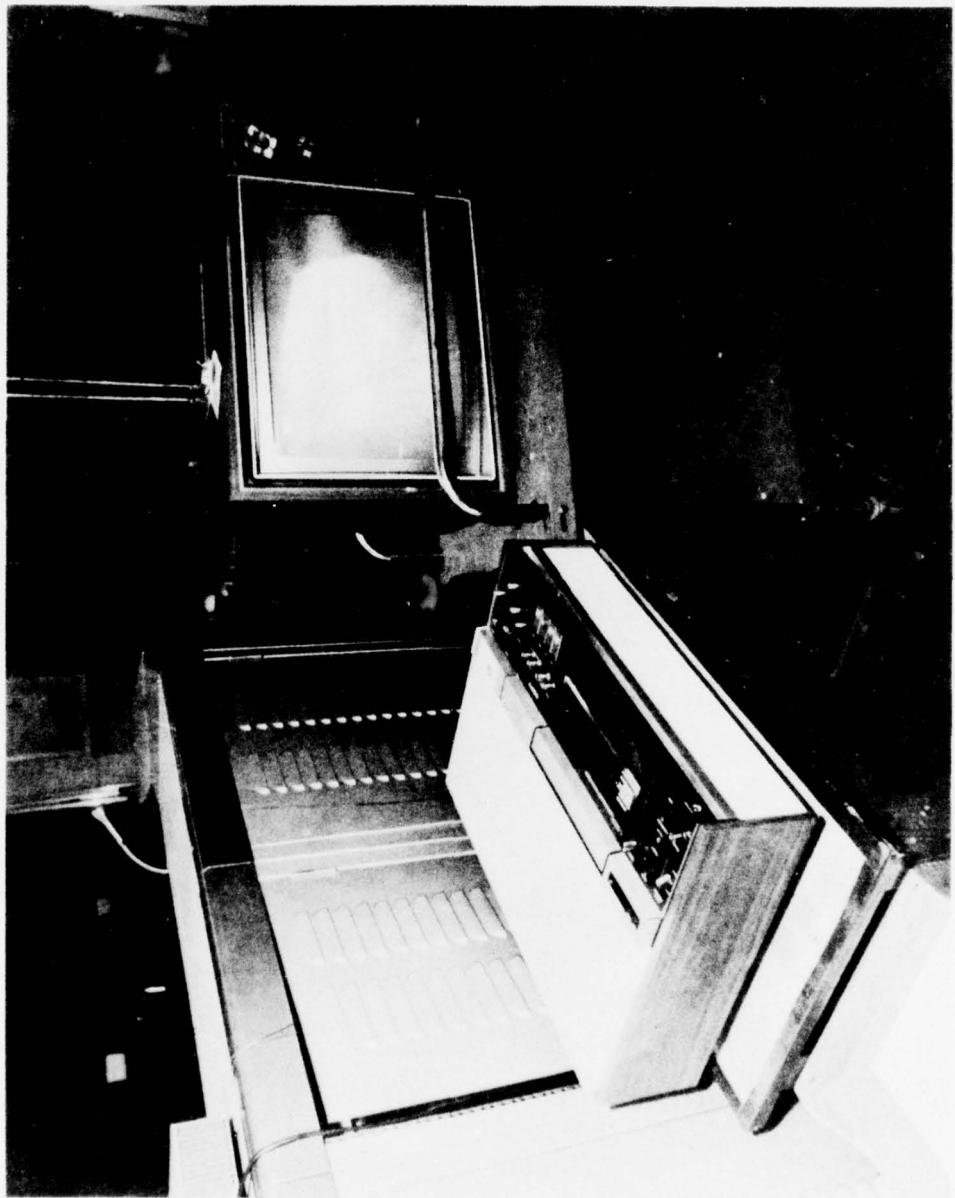
Figure 6. Video tape recorder with TV monitor.

The Schlieren and shadowgraph techniques will not be described in detail in this report. Numerous articles have been published on these standard methods [4, 5].

b.   Exposure and Processing of Interferometer Holograms

Shearing interferometers may be designed in a variety of configurations [6, 7]. In this case, we chose to make our own with holographic techniques. The interferometer is made up of one or two bleached Fourier transform holograms. The geometry for construction of the holograms is shown in Figure 7. A 15-mW helium-neon laser beam passes through a 50% beamsplitter cube. The two beams formed are each directed toward a spatial filter aimed at the holographic plate. One beam is attenuated by a 30% transmission filter. Using 4-in by 5-in. Agfa-Gevaert plates, exposure time was approximately 1 to 2 sec for a combined beam intensity of 5×10^{-5} W/cm^2. The resulting hologram was developed and bleached in a solution of potassium ferricyanide. Table 1 is a summary of developing and bleaching procedures. A diffraction efficiency of 20% was achieved in first order using this routine.
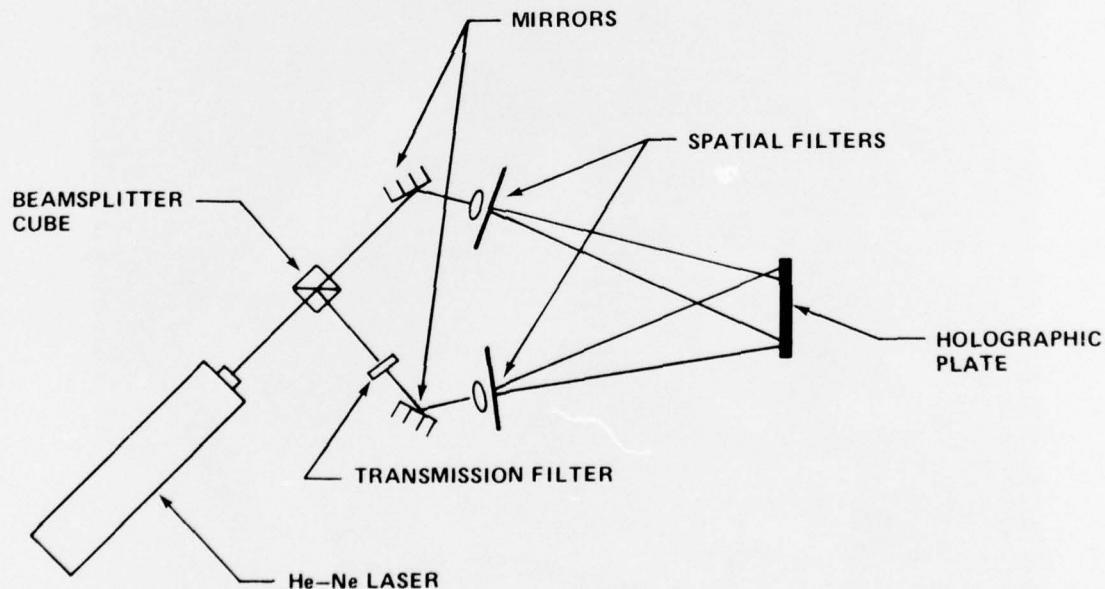
Figure 7. Hologram forming geometry.

8

TABLE 1. PROCESSING OF HOLOGRAMS

Plate	Agfa-Gevaert 10E75, 4 in. $\times$ 5 in. plate
Exposure	1-3 sec for incident beam irradiance of 5×10^{-5} W/cm^2
Development	D-19 or Dk-50 diluted 1/5 normal strength for 1 min or until plate is N.D. 1
Fix	1 min
Bleach	5% potassium ferricyanide solution, 2 min
Wash	Photoflow rinse, 3 min
Dry	20 min

An interferometer may be made from one or two plates. A double frequency hologram on one plate is made by either rotating or translating the exposed plate and taking an additional exposure [8]. A similar effect is achieved by taking each exposure on separate plates. The plates are placed emulsion to emulsion to form the interferometer, this configuration having a greater diffraction efficiency than a single plate.

c. Operation and Types of Holographically Constructed Lateral Shearing Interferometers

Figure 8 illustrates the concept of lateral shearing interferometry. An incident circular cross-section test beam originating from the left illuminates two holograms having a slightly differing dispersion ($\theta_1 \neq \theta_2$). A viewing screen placed in the diffracted beams will show a finite fringe pattern in the overlap of the beams. This is the principle of operation of the lateral shearing interferometer — a test beam being "slipped" and interfering with itself. The arbitrary amount that the test beam is slipped with itself determines the shear. Large overlap gives a low shear; a small overlap, large shear. Figure 9 shows the result of a small phase distortion in the test beam and the resulting perturbation of the fringes.

A few of the types of lateral shearing interferometers which could be used for either lens, mirror, or flow visualization testing is shown schematically in Figure 10. Either lens testing or flow visualization is pictured. Case (a) gives a variable shear using two plates, the shear proportional to the plate spacing [9]. This case has been discussed with Figure 8. Case (b) is used in a convergent wavefront, each hologram having a differing dispersion to give two diffracted beams having a common focus. Case (c) is a dual frequency grating requiring a double exposure on a single plate. Two plates placed emulsion to emulsion with the same dispersion (such as used in this report) would be equivalent to this case.

9
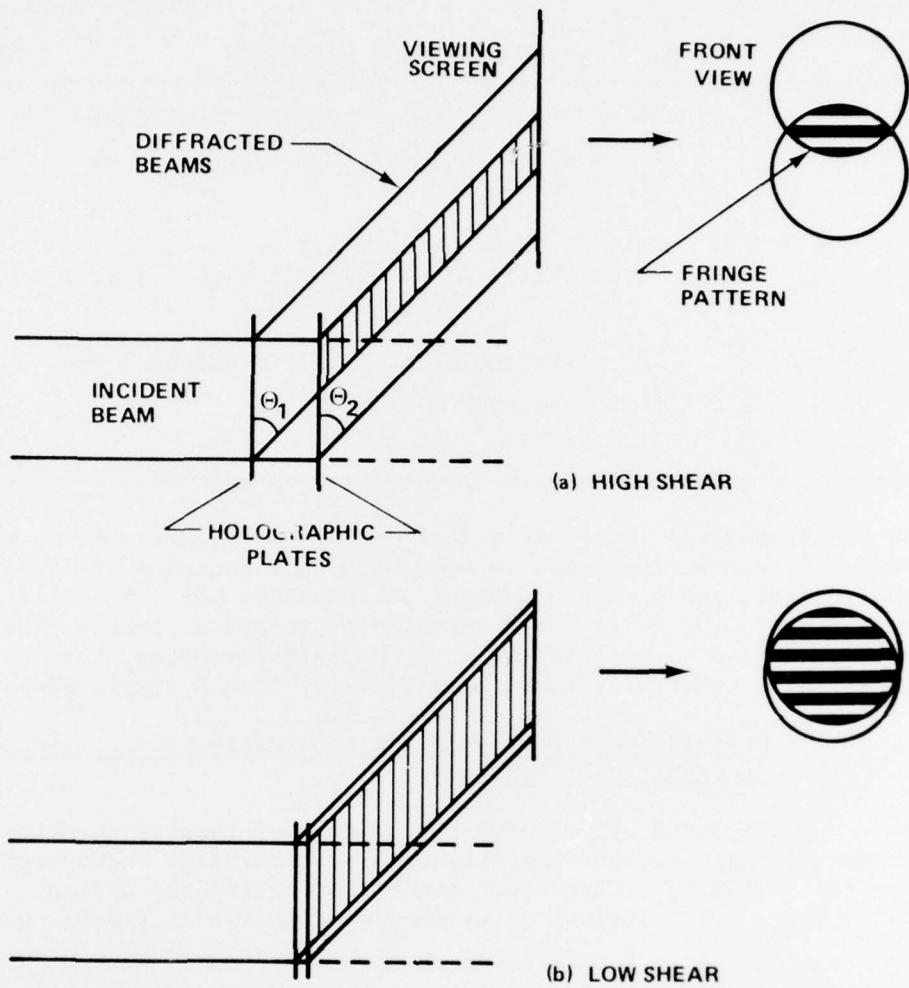
Figure 8. A lateral shearing interferometer.
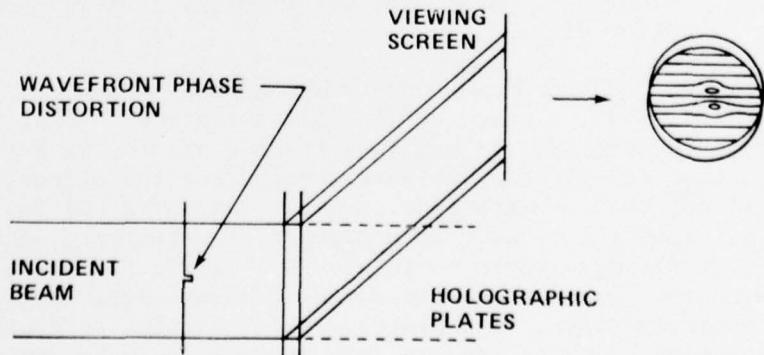
Figure 9. Shearing interferometer detecting a wavefront distortion.
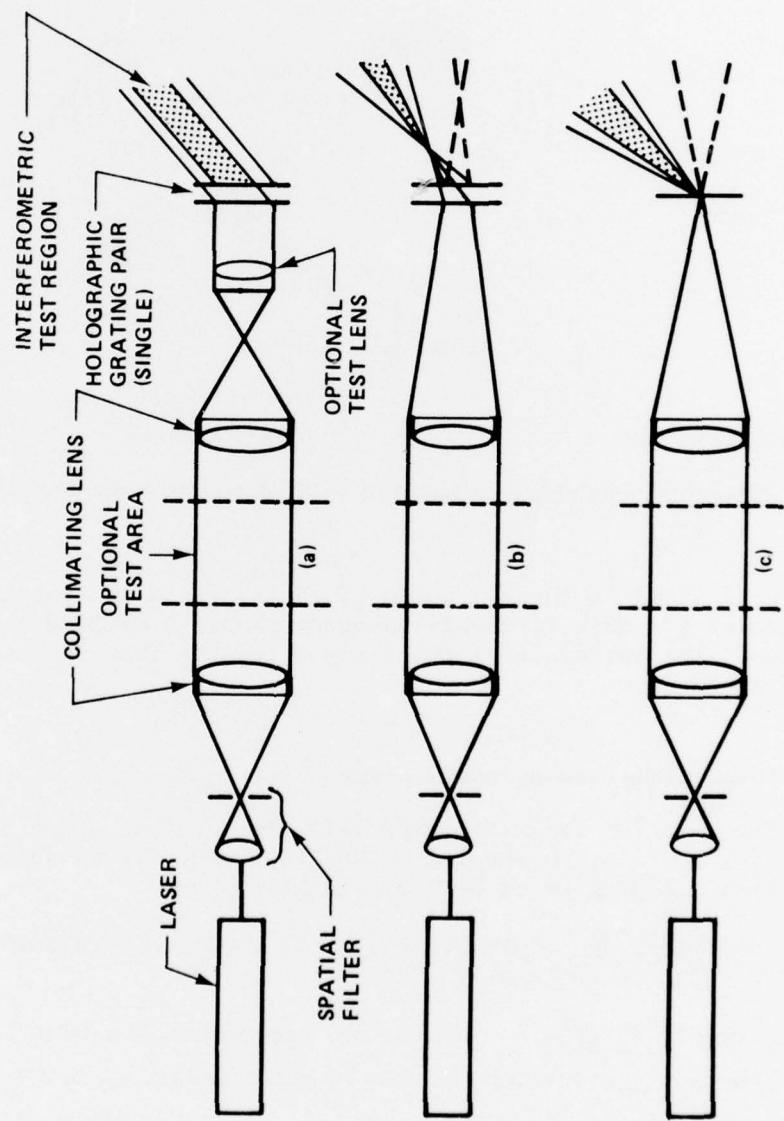
Figure 10. Examples of holographic lateral shearing interferometers.

11

Fringe formation in a convergent beam of Case (c) is shown in Figure 11. An infinite fringe is produced when the grating is at the focus of the beam. This results from the diffracted beams having the same Gaussian reference sphere. A small displacement of the grating along the optical axis gives a finite fringe pattern. The diffracted beams no longer originate at the same point and a wavefront tilt between the two beams is introduced.
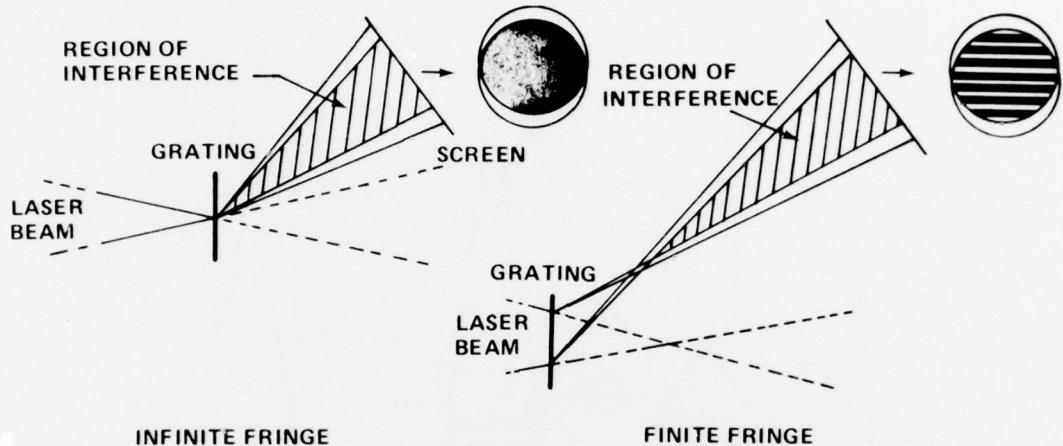
Figure 11. Fringe formation with a convergent beam.

Figure 12 shows an interferogram of an f/5.7, 10-in. paraboloid mirror taken with a dual frequency hologram placed a small distance inside focus. The curvature of the fringes results from the nonspherical surface of the mirror.

3.   Theory of the Shearing Interferometer

The shearing interferometer will yield unique solutions to an arbitrary wavefront. A general method for reduction of shearing interferograms has been given by Saunders [10].

A set of reference points are chosen as shown in Figure 13(a) with a separation equal to the amount of shear.

In Figure 13, P_v ($v = 0, 1, 2 \ldots N$) represents the $(N + 1)$ reference points in one of the images, W, of the sheared wavefront and P'_v the corresponding points in the other image, W'. Let δ_v [Figure 13 (b)] equal to the deviation of the wavefront at P_v, from the corresponding point, T_v, on a reference circle, C, (to be chosen later), ϵ equals the
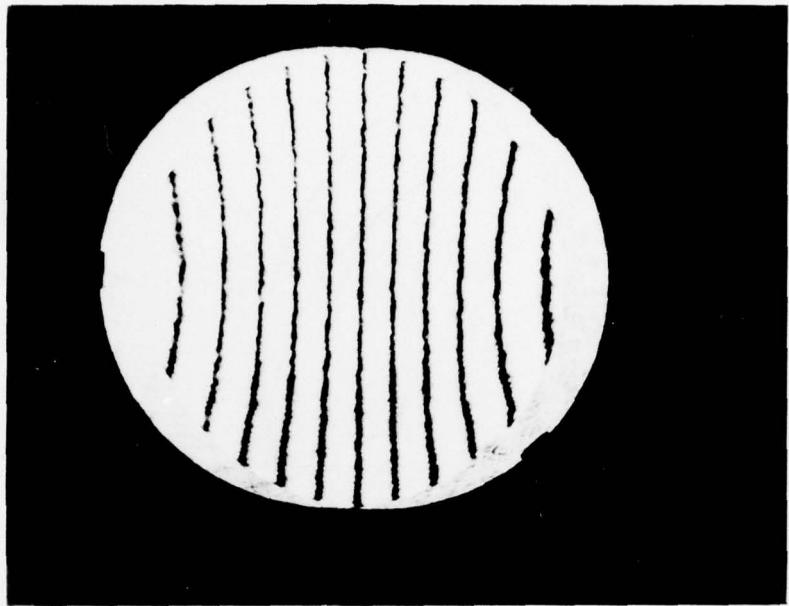
Figure 12. Interferogram of an f/5.7 paraboloid mirror.

angle between the two images, C and C', of the reference circle at their point of intersection, and μ equals the distance from the intersection point to P_0. The distance, μ, is positive if P_0 is below [Figure 13 (b)] the intersection of the two circles and negative if above. The deviation, δ_ν, is positive if P_ν is on the concave side of the circle, and negative if it lies on the convex side of the reference circle. The distance from P_0 to P_ν (or from T_0 to T_ν), measured along the circle, is always positive and is represented by ν.

The separation, S_ν (distance from T_ν to $T'_{\nu - 1}$), of the two images of the reference circle at any pair of points, P_ν and $P'_{\nu - 1}$, assuming unit shear) may be obtained from Figure 14. The centers of the two circles are located at C_1 and C'_1. The distance $C_1C'_1$ equals 2h, R equals the radii of the two circles, p equals the distance from E to T_ν, E bisects the line $C_1C'_1$ and ϕ is the angle subtended by $(\nu + \mu)$ at E. Applying the law of cosines (from trigonometry) to triangles $EC'_1T'_{\nu - 1}$ and EC_1T_ν we obtain

$$R^2 = h^2 + (p + S_\nu)^2 - 2h (p + S_\nu) \cos (90 - \phi)$$

$$R^2 = h^2 + p^2 - 2hp \cos (90 + \phi)$$

13
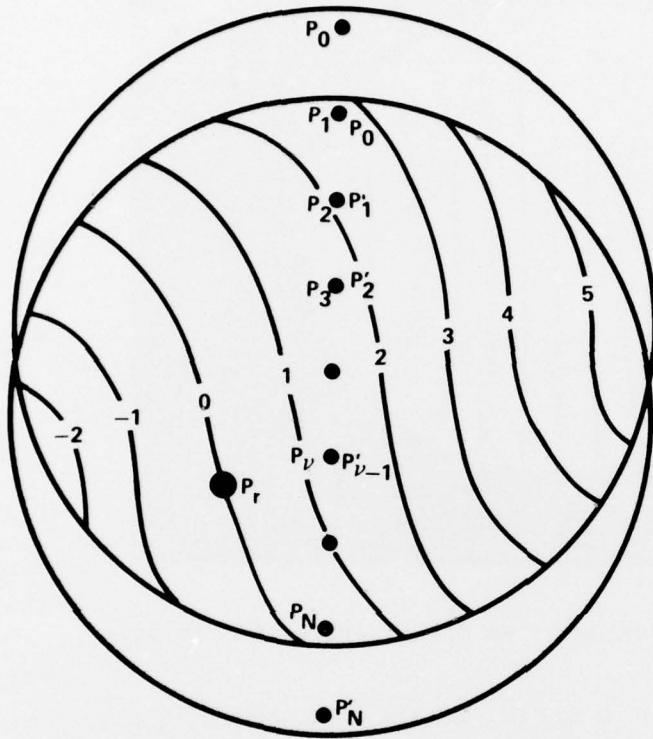
(a) Two images of a wavefront sheared laterally relative to itself.
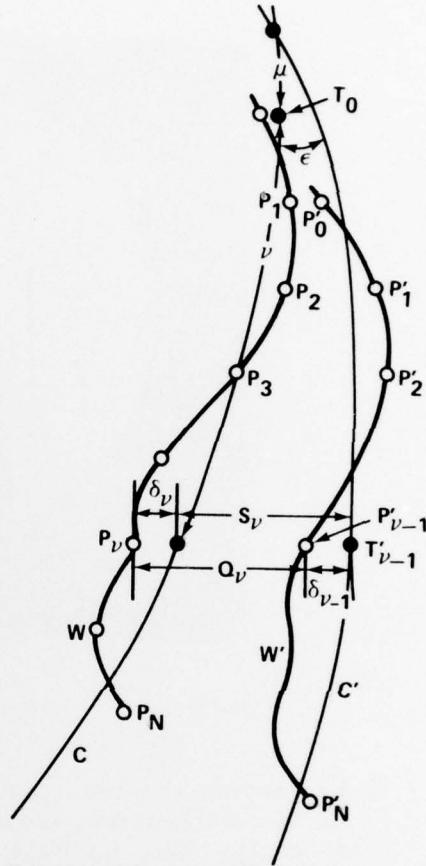
(b) Illustration of the two wavefronts relative to the images of a reference circle.

Figure 13. Schematic showing two images of a wavefront sheared laterally to itself and two wavefronts relative to the images of a reference circle.

On taking differences and solving for S_ν we obtain,

$$S_\nu = 2h \sin \phi \quad . \tag{1}$$

This equation may be applied rigorously, but if the focal ratio (radius of curvature of the circle divided by the diameter of the wavefront) exceeds six, no significant error is introduced by replacing $\sin \phi$ by its approximate equivalent, $(\nu + \mu)/R$. Also, since the angle ϵ will always be quite small, the value of $2h$ is approximately equal to $R \cdot \epsilon$ and the value of S_ν in Equation (1) becomes

$$S_\nu = (\nu + \mu) \epsilon \quad . \tag{2}$$

14
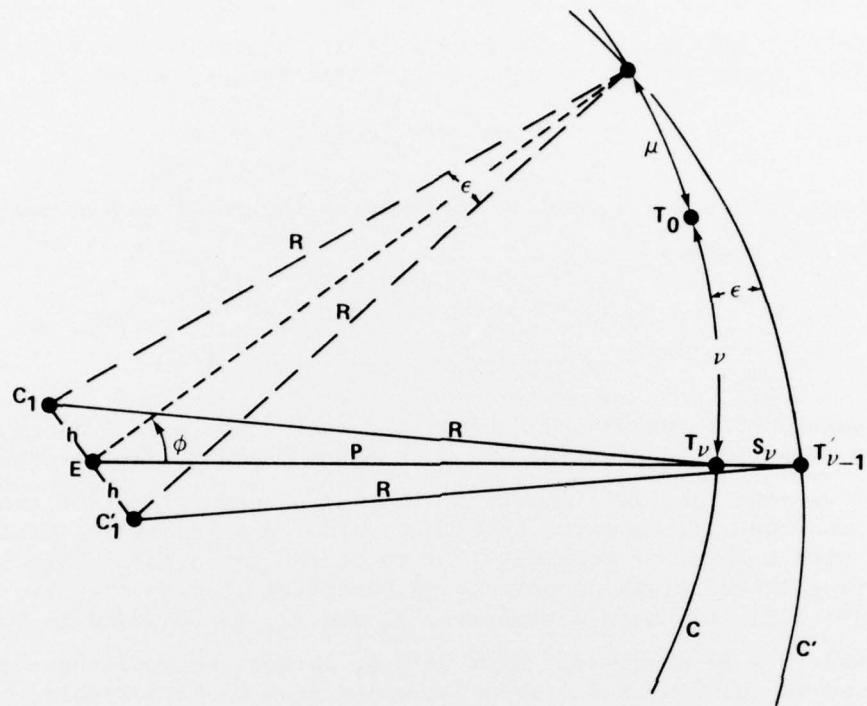
Figure 14. Relationship between parameters and other variables.

If we let Q_ν represent the separation of the two wavefronts, W and W', at P_ν, it is seen from Figure 13(b) that

$$\left. \delta_\nu = \delta_{\nu-1} + Q_\nu - S_\nu = \delta_{\nu-1} + Q_\nu - \epsilon (\nu + \mu) \right\} \quad . \quad (3)$$

$$\nu = 1, 2, 3 \ldots N$$

All quantities that represent optical distances are given in units of the wavelength that is used. Accordingly, these quantities should be multiplied by the wavelength to convert to standard units of length. The quantity Q_ν may be observed directly if white light is used to adjust the zero order to a known point, P_r, and then, using monochromatic light of known wavelength, observe the order difference between points P_r and P_ν. It is inconvenient and unnecessary to use white light. Let Q_r represent the unknown order of interference at an arbitrarily chosen point, P_r, in the fringe pattern [Figure 13(a)] and q_ν the difference in order (number of fringes) between this point and P_ν. The order of

15

interference, Q_ν, at P_ν is, therefore, equal to $(Q_r + q_\nu)$. This introduces another unknown into the equations of observation; but this may be replacing the product $\epsilon\mu$ with a new parameter, r, such that

$$\epsilon\mu = (Q_r - r) \quad . \tag{4}$$

With these values for Q_ν and $\epsilon\mu$ replaced by their respective equals, Equation (3) becomes

$$\left.\begin{array}{l} \delta_\nu = \delta_{\nu-1} + q_\nu + r - \nu\epsilon \\ \nu = 1, 2 \ldots N \end{array}\right\} \quad . \tag{5}$$

Equation (5) represents N equations that contain $(N + 3)$ unknowns: namely, $(N + 1)$ δ_ν's plus the two parameters ϵ and r. We need three additional equations relating these $(N + 3)$ unknowns if a solutions is to be possible. It appeared that one could use a second set of fringes formed with a shear of two units, as shown in Figure 13a. This would yield $(N - 1)$ additional equations of observations with only two new unknowns; i.e., two more parameters, ϵ_2 and r_2, to be added to the before-mentioned $(N + 3)$ unknowns. If N is 6 or larger, we would have as many equations as unknowns and a solution would seem to be possible, but it can be shown that these equations are not entirely independent.

The δ_ν's do not have significance until the reference circle, C, shown in Figure 13(b), is defined. Any circle may be defined by three conditions. In analytical geometry, these might be the coordinates of the center and the radius of the circle. A circle might also be defined as the one that passes through three given points. The circle of reference may be fully defined by three equations of condition. When these are combined with the set of observation equations [Equation (5)] data from a single set of fringes is sufficient for a complete solution.

The values of the deviations may be obtained without knowing the value of R. However, when testing a parabolic mirror, for instance, the deviations represent the difference between the parabola and a sphere. If comparison is to be made between the measured deviations of the wavefront and the computed deviations of a parabola from a circle, the radius of curvature of the circle must be known. The radius, R, can be measured independently of the interferometer. The ideal image point, E, (Figure 14) or the mean point of convergence of the wavefront, can be located and its distance from any chosen point can be measured directly. The center of the reference circle will be located at the ideal image point if the reference circle is chosen as the circle that best fits the observed wavefront. This may be done most precisely by the method of least squares. The value of R is the measured distance from the ideal image point (point of convergence) to any chosen reference point plus the computed deviation of this reference point from the reference circle.

16

In the test of a concave mirror, R is approximately equal to the radius of the mirror. In the test of a lens (simple or compound system), R is the distance from the point of convergence (image point) to the back surface of the lens.

Three methods for defining the reference circle of "best fit" for an arbitrary wavefront are mentioned by Saunders [10]. In the flow field studies outlined in this report, the reference sphere is defined by an interferogram taken of the cavity prior to each flow test.

4.   Test Results and Calculations

The interferogram of Figure 15 was taken during the steady-state portion of a test run. The cavity shrouds were set at an angle of 6°. The test parameters are given in Table 2. These results are compared to a previous test under similar conditions in which mirrors replaced the windows and closed cavity laser power was measured.

Data reduction of Figure 15 was accomplished in the following manner. An unperturbed interferogram was taken immediately before the test having the same coordinate system and magnification as Figure 15. A series of reference points equal to the shear displacement and along the shear direction (chosen along the y-axis) were placed on both interferograms. The fringe order at these points were measured, the fringe order at each point on the unpertrubed interferogram being subtracted from the order at an equivalent point on Figure 15. These deviations were summed parallel to the y-axis for each series of reference points.

Phase plots along y at arbitrary x-positions downstream of the nozzle exit were obtained. The data were then converted into isophase contours of Figure 16. Since the shear was taken along the y-axis, this figure represents phase distortions only in the y-direction. A maximum phase difference $\triangle\phi$ of 2.6 at the illumination wavelength of 6328 $\overset{\circ}{A}$ was calculated. This represents a far-field intensity degradation in the central lobe, I/I_o of 0.95 at 10.6 microns.

Figures 17, 18, and 19 are included for comparison. Figure 17 shows an interferogram of a few (3) fringes across the cavity, Figure 18 a transients in the chemical laser cavity. Similar details of shock structure are seen in all three views.

5.   Summary

The simplicity of construction and use of the lateral shearing interferometer lends itself readily to the measurement of flow properties. The standard interferometers in this field — Michelson, Twyman-Green, and Mach-Zehnder - all require a reference beam to interfere with the test beam. This introduces problems with movements of optical

TABLE 2. TEST CONDITIONS

| Test | Flow Rates (g/sec) | | | | | | Combustor Pressure (psia) | Cavity Pressure (torr) | Closed Cavity Power (kW) | Diffuser Exit Pressure (torr) |
	Total F_2	Secondary H_2	Combustor Products	CO_2	D_2	Total He				
CL-1367	30.5	1.07	51.9	45.1	17.5	71.5	33.6	31.7	—	89.1
CL-1178	29.1	1.02	50.4	46.4	17.1	71.4	34.3	32.6	2.03	88.89
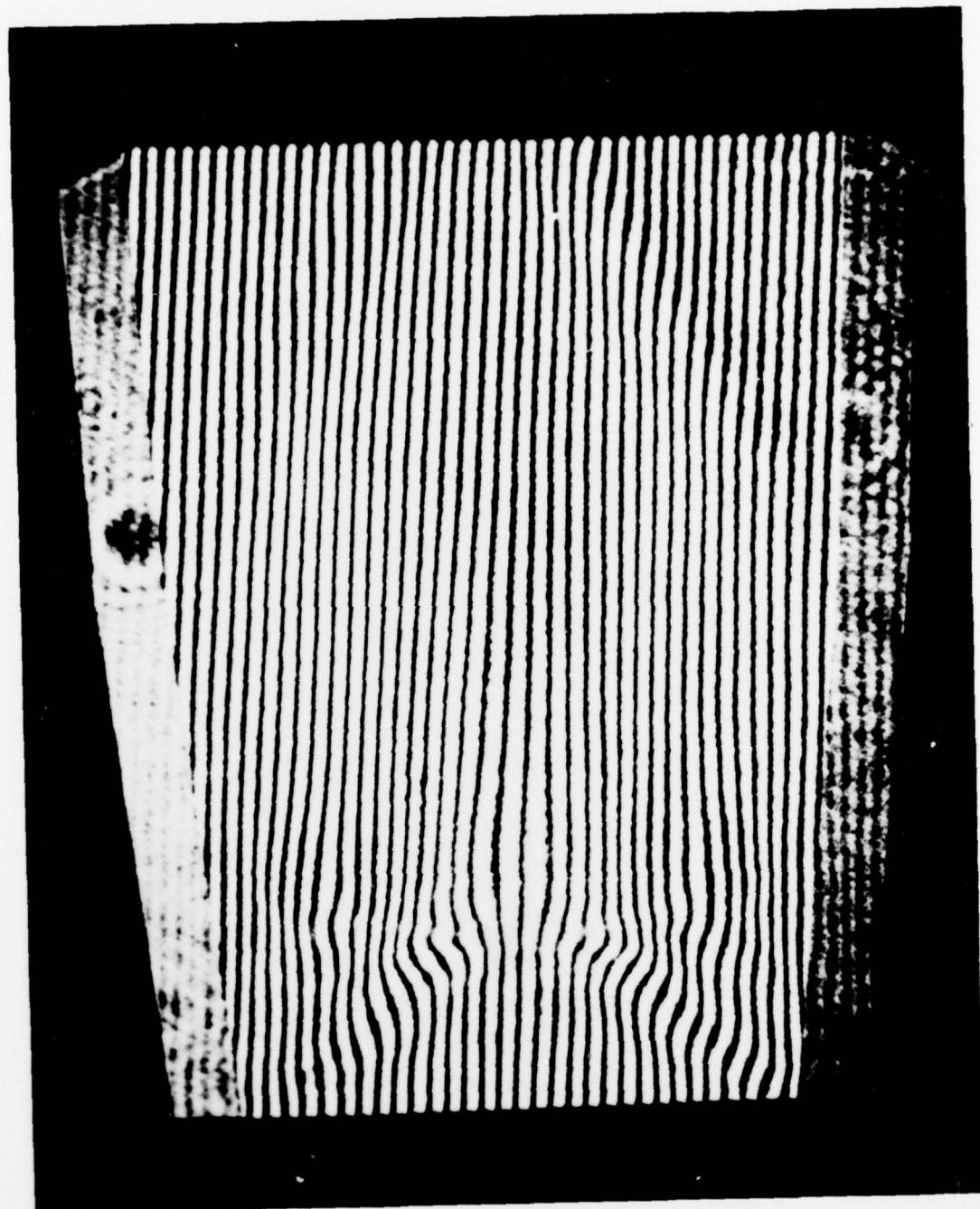
Figure 15.   Finite fringe interferogram of chemical
laser test CL-1367.

19
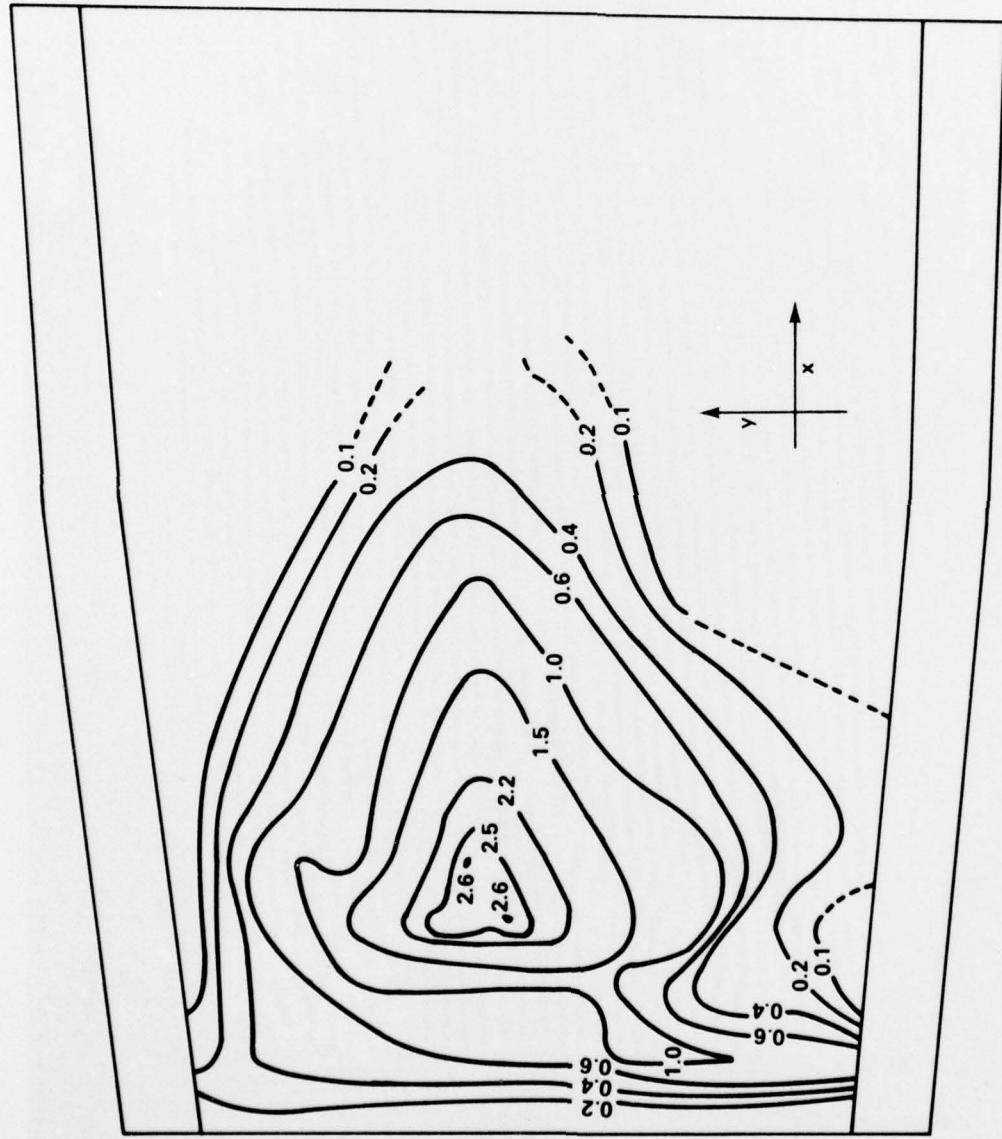
Figure 16. Phase contours obtained from Figure 15. (Obtained at 0.6328 μ wavelength, sensivity along y.)

Figure 17. Three fringe shearing interferogram.

21

Figure 18. Many fringe shearing interferogram.

Figure 19. Schlieren taken under similar test conditions of Figures 17 and 18.

components during an interferogram exposure — motions of a fraction of a wavelength are intolerable. The shearing interferometer, however, is relatively insensitive to vibrations because of its method of producing fringes.

The drawback of the shearing interferometer is in data reduction (the fringe pattern requires extensive manipulation to arrive at a final plot of phase). Additionally, two interferograms of the same test with orthogonal shear must be made for a complete description of the test wavefront.

REFERENCES

1. Connaughton, J. W. et al., <u>Chemical Laser Test Bed With Movable Wall Diffuser</u>, US Army Missile Command, Redstone Arsenal, Alabama, October 1975, Report No. RK-76-7 (Unclassified).

2. Lemke, Don, <u>Integral Combustor for a Chemical Laser</u>, Aerojet Corporation, 20 September 1974, Report No. TR-2091-001, (Unclassified).

3. Viecelli, J. J. et al., <u>Fine Orifice Injector Development</u>, Rocketdyne Division of Rockwell International Corporation, November 1974, Report No. RK-CR-75-22 (R-9616) (Unclassified).

4. Merzkrich, Wolfgang, <u>Flow Visualization</u>, Academic Press, New York, 1974.

5. Trolinger, J. D., <u>Laser Instrumentation for Flow Field Diagnostics</u>, NATO Advistory Group for Aerospace Research and Development, March 1974, Report No. AGARD-AG-186 (Unclassified).

6. Bates, W. J., "A Wavefront Shearing Interferometer," <u>Proc. Phys. Soc. Lon.</u>, Vol. 59, 1947, p. 940.

7. Saunders, J. B., <u>Jap J. Appl. Phys.</u>, Vol. 4, 1965, p. 94.

8. Wyant, J. C., "Double Frequency Grating Lateral Shear Interferometer," <u>Applied Optics</u>, Vol. 12, 1973, p. 2057.

9. Heriharan, P. and Hegedus, Z. S., "Double Grating Interferometers II. Application to Collimated Beams," <u>Opt. Commun</u>, Vol. 14, 1975, p. 148.

10. Saunders, J. B., <u>J. Res. Nat. Bur. Stand</u>, Vol. 65B, 1961, p. 239.

DISTRIBUTION

No. of
Copies

Defense Documentation Center
Cameron Station
Alexandria, Virginia   22314   12

Commander
US Army Materiel Command
ATTN: DRCRD   1
        DRCDL   1
5001 Eisenhower Avenue
Alexandria, Virginia   22333

DRSMI-FR, Mr. Strickland   1
     -LP, Mr. Voigt   1
     -RH   1
     -RHS, R. William Jones   18
     -RHAD, W. Lavaughn Hales   8
     -R, Dr. McDaniel   1
         Dr. Kobler   1
     -RBD   1
     -RPR (Record Set)   1
          (Reference Copy)   1